

# Investigating Heterogeneity of Intracellular Calcium Dynamics in Anterior Pituitary Lactotrophs Using a Combined Modelling/Experimental Approach

M. Tomaiuolo\*, R. Bertram†, A. E. Gonzalez-Iglesias\* and J. Tabak\*

\*Department of Biological Science and Program in Neuroscience, Florida State University, Tallahassee, FL, USA.

†Department of Mathematics and Programs in Neuroscience and Molecular Biophysics, Florida State University, Tallahassee, FL, USA.

## Journal of Neuroendocrinology

Cell responses are commonly heterogeneous, even within a subpopulation. In the present study, we investigate the source of heterogeneity in the  $\text{Ca}^{2+}$  response of anterior pituitary lactotrophs to a  $\text{Ca}^{2+}$  mobilisation agonist, thyrotrophin-releasing hormone. This response is characterised by a sharp increase of cytosolic  $\text{Ca}^{2+}$  concentration as a result of mobilisation of  $\text{Ca}^{2+}$  from intracellular stores, followed by a decrease to an elevated plateau level that results from  $\text{Ca}^{2+}$  influx. We focus on heterogeneity of the evoked  $\text{Ca}^{2+}$  spike under extracellular  $\text{Ca}^{2+}$  free conditions. We introduce a method that uses the information provided by a mathematical model to characterise the source of heterogeneity. This method compares scatter plots of features of the  $\text{Ca}^{2+}$  response obtained experimentally with those made from the mathematical model. The model scatter plots reflect random variation of parameters over different ranges, and matching the experimental and model scatter plots allows us to predict which parameters are most variable. We find that a large degree of variation in  $\text{Ca}^{2+}$  efflux is a likely key contributor to the heterogeneity of  $\text{Ca}^{2+}$  responses to thyrotrophin-releasing hormone in lactotrophs. This technique is applicable to any situation in which the heterogeneous biological response is described by a mathematical model.

**Key words:** heterogeneity, calcium, lactotroph, mathematical model, sensitivity analysis.

### Correspondence to:

Maurizio Tomaiuolo, Department of Biological Science and Program in Neuroscience, Florida State University, Tallahassee, FL 32306, USA  
(e-mail: mtomaiuolo@bio.fsu.edu).

doi: 10.1111/j.1365-2826.2010.02061.x

Heterogeneity is at the core of biological systems. The presence of heterogeneity might be an important feature (1–3) but, from an experimental point of view, it makes it harder to understand the system. Within an organism, there are many different cell types and, within each cell type, there is considerable variation (4). In addition, there are multiple sources of heterogeneity, such as stochastic gene expression (5), different cellular stages (6) and variation in channel/receptor modulation/expression (7).

Modelling approaches to heterogeneity have traditionally focused on two main goals. One aims to construct models that can reproduce all behaviours observed in the experimental data (8, 9), whereas the other is concerned with understanding how the observed heterogeneity may contribute to the overall performance of a system (10, 11). Our approach is to use mathematical modelling to uncover the source of the heterogeneity.

We look at the responses of anterior pituitary lactotrophs to a  $\text{Ca}^{2+}$  mobilising agonist as a case study. It is widely recognised that these cells are very heterogeneous (12–17). Such variability is expressed in terms of electrical activity (18, 19),  $\text{Ca}^{2+}$  signalling

(17, 18, 20, 21), hormone secretion (18, 22) and responsiveness to regulatory hormones (18, 23–25). Specifically, we look at the cytosolic  $\text{Ca}^{2+}$  response to thyrotrophin-releasing hormone (TRH). This neurohormone mobilises  $\text{Ca}^{2+}$  from the endoplasmic reticulum (ER) via activation of the  $G_q$  signalling pathway (26). The intracellular  $\text{Ca}^{2+}$  response consists of an initial spike and a subsequent plateau phase (26). The spike phase corresponds to rapid  $\text{Ca}^{2+}$  mobilisation from the ER, causing a transient increase of  $\text{Ca}^{2+}$  in the cytosol that is followed by a decay in the cytosolic  $\text{Ca}^{2+}$  concentration. The plateau phase is characterised by  $\text{Ca}^{2+}$  influx through voltage-dependent and -independent  $\text{Ca}^{2+}$  channels (27). To facilitate the analysis, we focus solely on heterogeneity in the spike phase, by applying TRH in the absence of extracellular  $\text{Ca}^{2+}$  to remove the plateau. First, we show that the spike response is very heterogeneous across the cell population, although the response of each cell is self-consistent during the course of the experiment. We then use a mathematical model of the spike response combined with sensitivity analysis to examine the source of heterogeneity.

Sensitivity analysis is often used to study the robustness of a model to variation in parameter values. That is, a parameter in the model is varied and the effect on the output is monitored. Although very useful in the analysis of the model, this type of manipulation is rarely possible in an experimental context. Instead, in the present study, we use the heterogeneity in the  $\text{Ca}^{2+}$  response to TRH to identify relationships between the observables of the response, and then compare these relationships with those obtained from a population of model cells with different degrees of variation in each parameter. The comparison between experimental and model data is enhanced by the results of the sensitivity analysis, which provides us with a framework to interpret these relationships. This approach can be extended to study other features of cells or cellular networks provided that a mathematical model exists for the system.

## Materials and methods

### Cell dispersion and lactotroph enrichment

Pituitary cell dispersion was conducted using papain/DNAse enzymatic digestion as previously described (28), pooling pituitary glands from several adult Sprague-Dawley pro-oestrus female rats. Anterior pituitary lactotrophs were enriched using a previously described protocol (29). Briefly, a Percoll-bovine serum albumin (0.3%) discontinuous density gradient was made by sequentially adding 2-ml layers of Percoll at densities of 70%, 60%, 50% and 35% (from bottom to top) to a 15-ml Falcon tube. Freshly dispersed anterior pituitary cells were placed on top of this gradient. After 30 min of centrifugation at 1500 g at room temperature, the cells at the interface between the 50% and the 35% layers were washed in medium 199 and centrifuged for 10 min at 600 g, resuspended, counted, plated on 1.5 glass bottom dishes (250 000 per dish), and cultured for 1 day in medium 199 with 10% foetal bovine serum. Viability of cells, determined by trypan blue exclusion, was always  $\geq 95\%$ . All cells in the lactotroph-enriched culture that responded to TRH were considered to be lactotrophs (28, 30).

### Calcium imaging

During each of the experiments ( $n = 12$ ), the field of view contained an average of 20 cells. The cells were rinsed once with HEPES-buffered saline (HBS) and then incubated in HBS containing  $2 \mu\text{M}$  of fura-2-AM (Molecular Probes, Carlsbad, CA, USA) for 45 min at room temperature. The cells were then rinsed three times with HBS, placed on the stage of an inverted microscope and continuously perfused with HBS at room temperature. TRH ( $10^{-7} \text{ M}$ ) was bath applied for periods of 1 min. Pairs of images were acquired every 2 s with a 12 bit charge-coupled device camera set to  $8 \times 8$  binning, controlled by TI WORKBENCH software developed by T. Inoue (Waseda University, Tokyo). The software also controlled the alternating illumination of the cells with 340- and 380-nm light beams.  $[\text{Ca}^{2+}]_i$  is expressed as the ratio of the intensity of the light emitted by cells after stimulation with 340 and 380 nm light ( $F_{340}/F_{380}$ ). We assumed that the ratio  $R = F_{340}/F_{380}$  was sufficiently far from the saturation portion of its curve to consider  $[\text{Ca}^{2+}]_i$  to be a linear function of  $R$ .

### Data analysis

The data consist of time series of  $\text{Ca}^{2+}$  fluorescence imaging. For each cell's time series, we first subtracted the average  $\text{Ca}^{2+}$  level so that each response had a baseline  $\text{Ca}^{2+}$  level of zero and then we computed three measures:

the peak, the decay rate and the area under the curve. The decay rate was computed by fitting an exponential decay function to each time series. The analysis was performed in Matlab (The Mathworks, Natick, MA, USA). The code used for the analysis is available elsewhere (<http://www.math.fsu.edu/~bertram/software/pituitary>).

### Two-compartment model

We use a two-compartment model (31) that describes the dynamics of calcium concentration in the cytosol and in the ER (Fig. 1).

This model contains the essential elements for  $\text{Ca}^{2+}$  dynamics in pituitary cells. The concentration of  $\text{Ca}^{2+}$  in the cytosol is a function of  $\text{Ca}^{2+}$  flux across the plasma membrane ( $J_{\text{mem}}$ ) and the ER membrane ( $J_{\text{er}}$ ). The differential equation for the concentration of free cytosolic  $\text{Ca}^{2+}$  ( $\text{Ca}$ ) is:

$$\frac{d\text{Ca}}{dt} = f_c(J_{\text{mem}} - J_{\text{er}}) \quad (1)$$

where  $f_c$  is the fraction of free cytosolic  $\text{Ca}^{2+}$ , and:

$$J_{\text{mem}} = J_{\text{in}} - J_{\text{out}}. \quad (2)$$

To replicate the experimental conditions, we set the rate of  $\text{Ca}^{2+}$  influx to zero (i.e.  $J_{\text{in}} = 0$ ) but we retain  $J_{\text{in}}$  temporarily during the development of the reduced model. The  $\text{Ca}^{2+}$  efflux ( $J_{\text{out}}$ ) results from the combined action of plasma membrane  $\text{Ca}^{2+}$ -ATPase pumps and  $\text{Na}^+$ - $\text{Ca}^{2+}$  exchangers. Previous findings suggest that the exchangers play a minor role (32), so we do not include them in the model. The plasma membrane  $\text{Ca}^{2+}$  pump rate is assumed to be linear:

$$J_{\text{out}} = k_{\text{pmca}}\text{Ca} \quad (3)$$

where  $k_{\text{pmca}}$  is the constant pump rate.

The concentration of  $\text{Ca}^{2+}$  in the ER ( $\text{C}_{\text{er}}$ ) is a function of  $\text{Ca}^{2+}$  flux through the ER membrane and is described by:

$$\frac{d\text{C}_{\text{er}}}{dt} = f_{\text{er}}\nu J_{\text{er}} \quad (4)$$

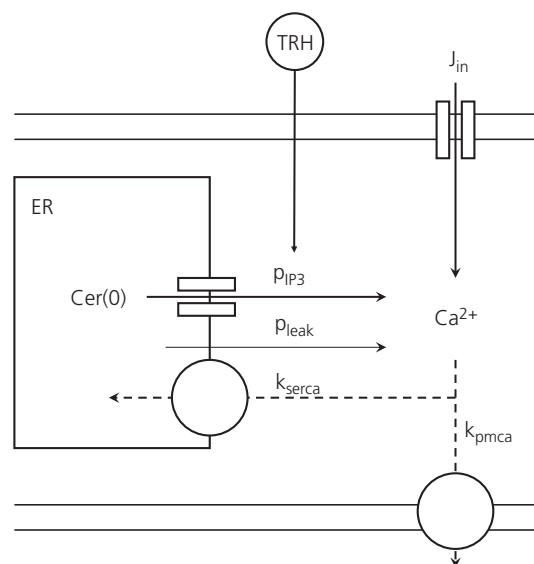


**Fig. 1.** Representation of the simplified model of  $\text{Ca}^{2+}$  dynamics. Each  $\text{Ca}^{2+}$  flux is represented by an arrow with the corresponding parameter name. Parameter values and definitions are provided in Table 1. ER, endoplasmic reticulum; TRH, thyrotrophin-releasing hormone.

where  $f_{er}$  is the fraction of free  $Ca^{2+}$  in the ER, and  $v$  is the ratio of the cytosolic to the ER volume ( $v_c/v_{er}$ ). We model the flux through the ER membrane as:

$$J_{er} = J_{serca} - J_{ip3} - J_{leak}. \quad (5)$$

Here,  $J_{serca}$  describes the flux through sarco/endoplasmic reticulum  $Ca^{2+}$ -ATPase pumps (SERCA), whereas  $J_{leak}$  and  $J_{ip3}$  describe the flux from the ER into the cytosol as a result of leakage and inositol trisphosphate ( $IP_3$ ) receptor/channel permeability. These are described by:

$$J_{serca} = k_{serca}Ca \quad (6)$$

$$J_{leak} = \rho_{leak}(C_{er} - Ca) \quad (7)$$

$$J_{ip3} = \rho_{ip3}(C_{er} - Ca) \quad (8)$$

where  $k_{serca}$  represents the SERCA pumps rate (we assume a linear pump flux), and  $\rho_{leak}$  and  $\rho_{ip3}$  are the flux rates through leakage and  $IP_3$  channels, respectively. All parameter values are listed in Table 1. The differential equations were solved numerically (Fig. 2) using the Runge-Kutta fourth order method in XPPAUT (33).

**Table 1.** Default Parameter Values.

Parameter	Value	Definition	Units
$f_c$	0.01	Fraction of free cytosolic calcium	
$f_{er}$	0.01	Fraction of free ER calcium	
$N$	30	Ratio of cytosol to ER volume	
$\rho_{leak}$	0.0002	Leakage from ER into the cytosol	$ms^{-1}$
$\rho_{ip3}$	0.004	Rate of $IP_3$ channels flux	$ms^{-1}$
$C_{er}(0)$	132	Initial concentration of calcium in the ER	$\mu M$
$k_{pmca}$	0.15	Plasma membrane pump rate	$ms^{-1}$
$k_{serca}$	0.3	SERCA pump rate	$ms^{-1}$

ER, endoplasmic reticulum;  $IP_3$ , inositol trisphosphate; SERCA, sarco/endoplasmic reticulum  $Ca^{2+}$ -ATPase pump.

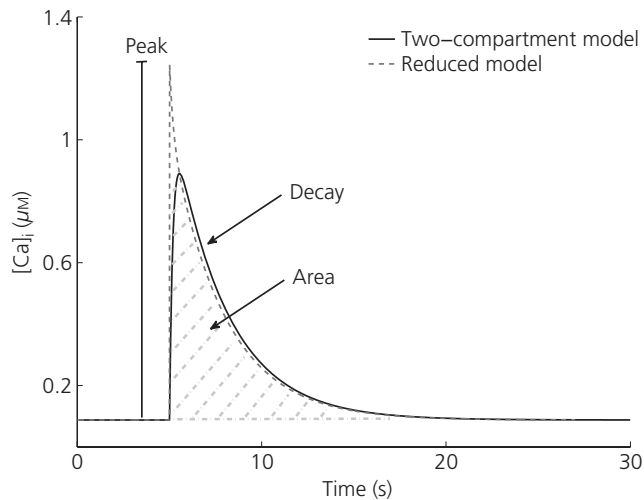


**Fig. 2.** Comparison of the two-compartment (solid line) and the reduced (dashed line) model. The features measured in the model and experimental data (peak, decay rate and area) are also illustrated.

## Model reduction

Here, we use the rapid equilibrium approximation to simplify the model and obtain formulae for some features of interest. This technique makes use of the fact that, if two variables change on very different time scales, the faster one can be approximated by its equilibrium value. In our model, this is the case for the cytosolic  $Ca^{2+}$  concentration, which changes much faster than the ER  $Ca^{2+}$  concentration (34). The rapid equilibrium approximation is obtained by setting Eqn (1) to zero and solving for the (quasi-equilibrium)  $Ca^{2+}$  concentration ( $Ca_{eq}$ ):

$$Ca_{eq} = \frac{J_{in} + (\rho_{leak} + \rho_{ip3})C_{er}}{k_{pmca} + k_{serca} + \rho_{leak} + \rho_{ip3}}. \quad (9)$$

By substituting  $Ca_{eq}$  for  $Ca$  in Eqn (4), we obtain:

$$\frac{dC_{er}}{dt} = f_{er}v[\omega J_{in} - (1 - \omega)(\rho_{leak} + \rho_{ip3})C_{er}] \quad (10)$$

with:

$$\omega = \frac{k_{serca} + \rho_{leak} + \rho_{ip3}}{k_{pmca} + k_{serca} + \rho_{leak} + \rho_{ip3}}. \quad (11)$$

Equation (10) is a differential equation that we can solve analytically provided that  $J_{in}$  is constant or piecewise constant, obtaining:

$$C_{er} = \left( C_{er}(0) - \frac{\lambda_1}{\lambda_2} \right) e^{-\lambda_2 t} + \frac{\lambda_1}{\lambda_2} \quad (12)$$

where  $C_{er}(0)$  is the initial concentration of  $Ca^{2+}$  in the ER. In our analysis, this would correspond to the point in time when TRH is applied. In addition:  $\lambda_1 = f_{er}v\omega J_{in}$ , and

$$\lambda_2 = \frac{f_{er}vk_{pmca}(\rho_{leak} + \rho_{ip3})}{k_{pmca} + k_{serca} + \rho_{leak} + \rho_{ip3}}. \quad (13)$$

The reduced model is thus composed of Eqns (9,12). To simulate the TRH response, we switch the value of  $\rho_{ip3}$  from zero to a positive value, instantaneously activating the  $IP_3$  channels and producing a cytosolic  $Ca^{2+}$  spike that then decays to its baseline concentration. The TRH response is thus reduced to an exponential decay from the peak  $Ca^{2+}$  value (Fig. 2).

Using the reduced model, we can derive analytical expressions for the same features that we measure from the experimental data: the peak of the  $Ca^{2+}$  response, the rate of decay and the area under the curve (Fig. 2). The peak of the  $Ca^{2+}$  response is computed from Eqn (9), increasing the  $IP_3$  channel flux rate from 0 to  $\rho_{ip3}$ :

$$\text{Peak} = \frac{J_{in} + (\rho_{leak} + \rho_{ip3})C_{er}(0)}{k_{pmca} + k_{serca} + \rho_{leak} + \rho_{ip3}}. \quad (14)$$

The peak increases with an increase of the  $IP_3$  channel flux rate ( $\rho_{ip3}$ ), the concentration of  $Ca^{2+}$  in the ER at the time of agonist application [ $C_{er}(0)$ ], the  $Ca^{2+}$  leakage rate ( $\rho_{leak}$ ) and the amount of  $Ca^{2+}$  influx ( $J_{in}$ ). The rate of decay  $\lambda_2$  is defined in Eqn (13) and is a function of several parameters. A quick investigation reveals that the decay rate increases with  $\rho_{ip3}$ ,  $\rho_{leak}$  and the rate of  $Ca^{2+}$  extrusion from the cytosol through the plasma membrane calcium pumps ( $k_{pmca}$ ). Finally, we compute the area under the response curve, as the integral of Eqn (9) assuming no  $Ca^{2+}$  influx ( $J_{in} = 0$ ), taken from the peak until  $Ca^{2+}$  returns to its baseline concentration, which simplifies to:

$$\text{Area} = \frac{C_{er}(0)}{f_{er}vk_{pmca}}. \quad (15)$$

Equation (15) reveals that the area is equal to the peak/decay rate, which is proportional to the concentration of  $[Ca^{2+}]_{ER}$  at the time of agonist application and inversely proportional to the rate of  $Ca^{2+}$  extrusion via

plasma membrane  $\text{Ca}^{2+}$  pumps. It is interesting that the area does not depend on the  $\text{IP}_3$  channel flux, although both the height of the peak and the decay rate do (Eqns 13,14). A larger  $J_{\text{IP}_3}$  increases the peak and produces a compensatory increase in the decay rate, so that the area is unchanged. The reduced model, Eqns (9,12), overestimates the peak response to a simulated application of TRH (Fig. 2). However, it retains the relationships between peak, decay rate, and area that are needed for comparisons with experimental data.

## Results

### Between-cell variation is larger than within-cell variation

The present study investigates the heterogeneity in the lactotroph response to TRH. First, we show that changes in cellular behaviour that emerge during the time course of the experiments do not contribute to heterogeneity. We recorded  $\text{Ca}^{2+}$  responses to a 1-min challenge of TRH (100 nM). Consecutive TRH applications were given 30 min apart to allow ER stores to replenish between applications (35). Each challenge of TRH was applied in the absence of extracellular  $\text{Ca}^{2+}$  (removed 5 min before and added back 5 min after TRH treatment), to prevent  $\text{Ca}^{2+}$  influx into the cell during the stimula-

tion. This removes one potential factor in the response heterogeneity. Figure 3(A) shows thirteen  $\text{Ca}^{2+}$  traces from individual lactotrophs responding to the same application, exhibiting considerable variability. By contrast, Fig. 3(B–E) shows traces from four different cells subjected to two consecutive TRH applications. In each cell, the response to the second TRH application was very similar to that of the first application. Thus, during the time course of our observations, there is heterogeneity in the TRH response between cells, although with uniformity of response within single cells to multiple TRH applications. This also shows that the observed heterogeneity is not a result of measurement noise.

### Single parameter sensitivity analysis

Between any two cells, there are many potential differences that could result in the heterogeneity of the  $\text{Ca}^{2+}$  response. Our goal is to determine where this variation is more likely to be found. For example, is variation in the rate of  $\text{Ca}^{2+}$  flux through SERCA a more likely source of measurable heterogeneity than variation in the flux through plasma membrane pumps or G-protein coupled receptor activities?

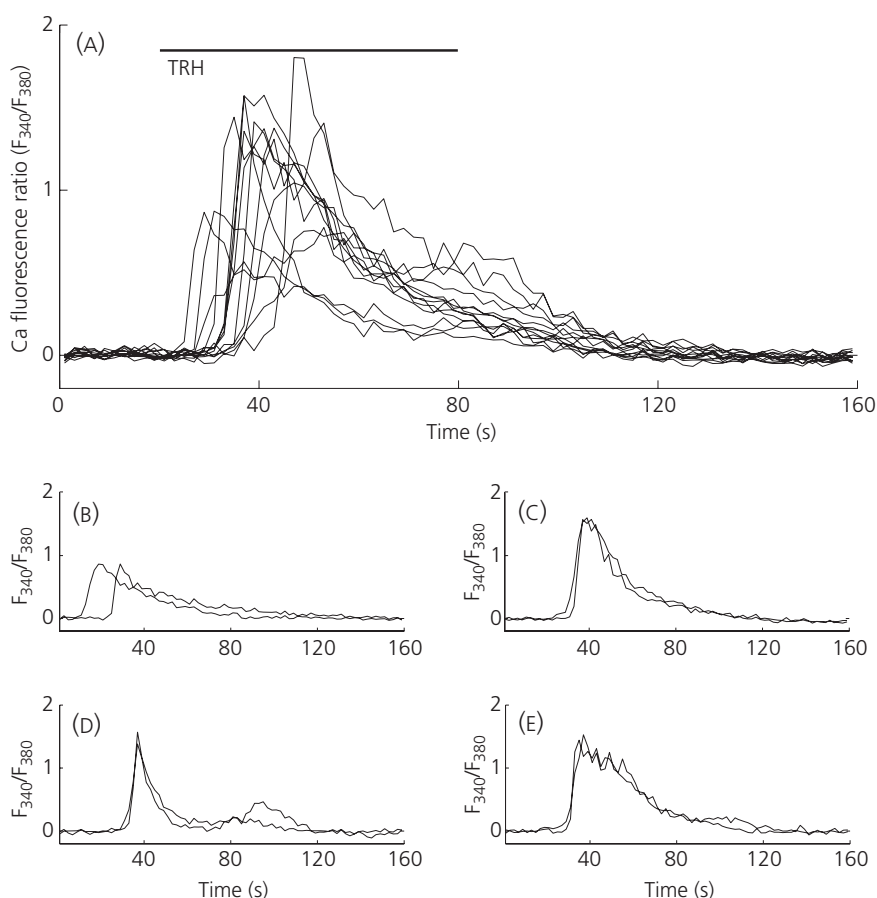


**Fig. 3.** Heterogeneity of the  $\text{Ca}^{2+}$  response to thyrotrophin-releasing hormone (TRH) in pituitary lactotrophs. In all panels, the x-axis shows time in seconds, and the y-axis shows the  $\text{Ca}^{2+}$  fluorescence ratio ( $F_{340}/F_{380}$ ). (A) Thirteen individual  $\text{Ca}^{2+}$  traces from the same experiment. Extensive variation exists in the peak, area, latency of response and decay rate. (B–E) Examples of single cell  $\text{Ca}^{2+}$  traces from the same experiment showing very similar responses to two successive challenges of TRH, 30 min apart.

Analysis of a mathematical model can help us address this question. The model described in the Materials and methods contains several parameters that represent factors such as SERCA or plasma membrane pump rates. One can study how variation in these parameter values affects a simulated response to TRH. This is the goal of sensitivity analysis, which determines how sensitive a model output is to changes in parameter values. Because we derived analytical expressions for the features we want to measure, we would not need to implement sensitivity analysis in the standard way (the formula for each feature could be plotted as a function of each parameter). We do it here to show the procedure that one would use in the more typical case where analytical expressions for the features cannot be obtained. We quantify the effects of parameter changes using the relative change (RC) in model output ( $y$ ) given a change ( $\Delta p$ ) in the parameter value ( $p$ ):

$$RC(p) = \frac{y(p + \Delta p) - y(p)}{y(p)}, \quad (16)$$

where  $\Delta p$  is the absolute change (positive or negative) in the default value of  $p$ . The relative change in  $p$  is then  $\alpha = \Delta p/p$ . For example, if  $\alpha = 0.1$  and  $RC(p) = 0.5$  then a 10% increase in the parameter corresponds to a 50% increase in model output. We simulate the TRH application with the model, and use the free cytosolic  $\text{Ca}^{2+}$  concentration (the Ca variable) time course to determine the peak, the decay rate and the area under the curve. Each of these features is used, separately, in Eqn (16) to calculate the sensitivity of the feature to changes in the various model parameters. In our

simulations, we changed the value of each parameter considered by as much as 70% of its default value.

We start by looking at the effects of changing the concentration of  $\text{Ca}^{2+}$  in the ER ( $[\text{Ca}^{2+}]_{\text{ER}}$ ) at the time of the simulated TRH application,  $C_{\text{er}}(0)$  (Fig. 4A). By increasing this parameter, we observe a positive linear effect on the peak and on the area (overlapping symbols), whereas there is no effect on the decay rate. Thus, increasing the initial  $[\text{Ca}^{2+}]_{\text{ER}}$  results in an increase of the peak and the area of the response. This happens because there is more  $\text{Ca}^{2+}$  available for release through the  $\text{IP}_3$  channels, increasing the peak of the response. Because the decay rate is unchanged, the area is increased as a result of the increase in the peak.

We next examine the effects of changing the parameter that describes the efficacy of the  $\text{IP}_3$  pathway ( $p_{\text{ip}3}$ ), determining the magnitude of the  $\text{Ca}^{2+}$  flux through activated  $\text{IP}_3$  channels subsequent to agonist binding to the TRH receptor. Variation in this parameter reflects the multiple events involved in the  $G_q$  signalling pathway, from the extent of receptor occupancy and coupling, to the number of  $\text{IP}_3$  receptors present on the ER membrane. Figure 4(B) shows that increasing  $p_{\text{ip}3}$  increases both the peak and the decay rate (overlapping symbols), whereas there is no effect on the area. Thus, the increase in the peak is exactly compensated by the increased decay rate, keeping the area constant. It is interesting that, although an increase in either  $C_{\text{er}}(0)$  or  $p_{\text{ip}3}$  increases the capacity for a robust response to stimulation, their effect on the three features are quite different. This reflects the fact that increasing  $C_{\text{er}}(0)$  increases the driving force for the

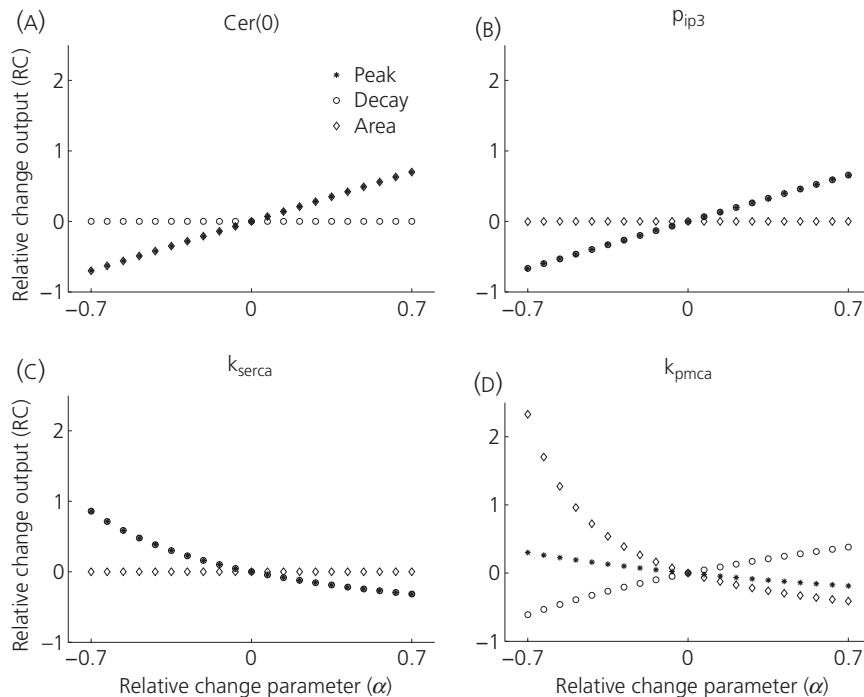


**Fig. 4.** Single parameter sensitivity analysis. In all panels, the x-axis shows the relative change in the parameter value, and the y-axis shows the corresponding relative change in output. (A) Changes in  $C_{\text{er}}(0)$  have identical effect on the peak and the area of the response but no effect on the decay rate. (B) Changes in  $p_{\text{ip}3}$  affect peak and decay rate in the same way but have no effect on the area. (C) Changing  $k_{\text{serca}}$  affects peak and decay rate in the same way but has no effect on the area. (D) Changes in  $k_{\text{pmca}}$  have different effects on all features.

**Table 2.** Summary of the Effects of Model Parameters on the Features.

Parameter	Peak	Decay rate	Area
$C_{er}(0)$	+	0	+
$\rho_{ip3}$	+	+	0
$k_{serE}$	-	-	0
$k_{pmca}$	-	+	-

A plus (minus) sign indicates that an increase (decrease) in parameter value results in an increase in the feature; a zero indicates that changing the parameter value has no effect on the feature.

response, whereas increasing  $\rho_{ip3}$  increases the permeability of the release pathway.

The effects of changing the SERCA pump rate are considered next ( $k_{serca}$ , Fig. 4c). Increasing this parameter decreases the peak and the decay rate (overlapping symbols), although it has no effect on the area. We observed the same property with changes in  $\rho_{ip3}$ , where variations in the peak and decay rate exactly compensate so that there is no change in the area.

Changes in the rate of cytosolic  $Ca^{2+}$  extrusion are shown in Fig. 4(d). A change in this parameter ( $k_{pmca}$ ) affects all of the features nonlinearly. An increase in  $k_{pmca}$  reduces the peak and the area but increases the decay rate. This happens because, by increasing  $k_{pmca}$ , we increase the rate at which  $Ca^{2+}$  is extruded from the cytosol, which in turn blunts the TRH response and accelerates the return of  $Ca^{2+}$  to the basal level.

It is clear that the different parameters have different effects on each of the features. For example,  $k_{serca}$  and  $k_{pmca}$  have opposite effects on the decay rate but similar effects on the peak, whereas  $\rho_{ip3}$  and  $k_{serca}$  have opposite effects on peak and decay rate but no effects on the area. A summary of the effects of each parameter on the measured features from the model output is presented in Table 2.

### Feature scatter plots

Using sensitivity analysis helps us to gain insight into a biological system, although it suffers from an inconvenient caveat: it cannot be directly applied experimentally. That is, we can change a parameter in the model by a desired amount and observe the effect that

it has on the output but we can rarely do the same in an actual experiment. We can, however, use the information gained from sensitivity analysis in a different way.

First, we construct scatter plots of the measured features from experimental data. The results from one experiment are shown in Fig. 5. One can, for example, construct a plot of all the peaks against all the decay rates, or all the peaks against all the areas, and so forth. In the example shown, there is no correlation between decay rate and peak (Fig. 5A), a strong positive correlation between area and peak (Fig. 5B) and a negative correlation between decay rate and area (Fig. 5C). In these scatter plots, we standardise the data; thus, for example, a peak of two corresponds to a peak that is two standard deviations from the mean of the experiment [i.e.  $(x-\mu_x)/\sigma_x = 2$ ].

Now, using the model, we can construct a plot similar to the scatter plot made with experimental data by varying one or more parameters. We can then compare the plots resulting from the experimental data to those obtained from the simulations to gain insight into which parameter(s) is most likely responsible for the response variability in the cell population.

We begin by examining model scatter plots obtained by changing one parameter at a time (Fig. 6, arrows indicate direction of parameter increase). Figure 6 is constructed using the same model results as Fig. 4 but plotted in a different way. Figure 6(A) shows the scatter plot between the decay rate and the peak. Changes in  $k_{serca}$  and  $\rho_{ip3}$  both result in a positive correlation between peak and decay rate. That is, variations (positive or negative) in either parameter produce points on a curve with positive slope in the decay rate-peak plane. This is clear from inspection of the expressions for decay rate (Eqn 13) and peak (Eqn 14). The  $k_{serca}$  (or  $\rho_{ip3}$ ) parameter appears in the same position in each equation; thus, changing this parameter will affect these two features in a similar way. Changes in  $k_{pmca}$  result in a negative correlation between peak and decay rate. This happens because in the expressions for these two features  $k_{pmca}$  appears in the numerator of one (Eqn 13) and in the denominator of the other (Eqn 14), so an increase in one corresponds to a decrease of the other. Changes in  $C_{er}(0)$  have no effect on the decay rate but have a large effect on the peak because  $C_{er}(0)$  only appears in the numerator of the peak equation (Eqn 14). Taken together, these observations indicate that in the decay rate-peak feature space variations in different parameters produce very different patterns; some patterns have positive slope, some have

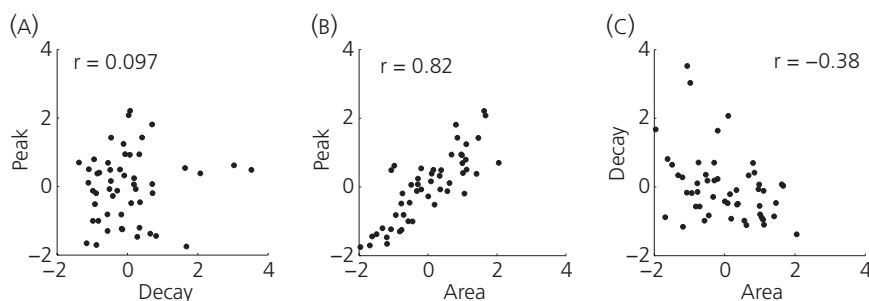


**Fig. 5.** Experimental data scatter plots constructed from one experiment. The data for each feature have been standardised (see text). (A) No correlation exists between peak and decay rate. (B) There is a positive correlation between peak and area. (C) There is a negative correlation between area and decay rate.

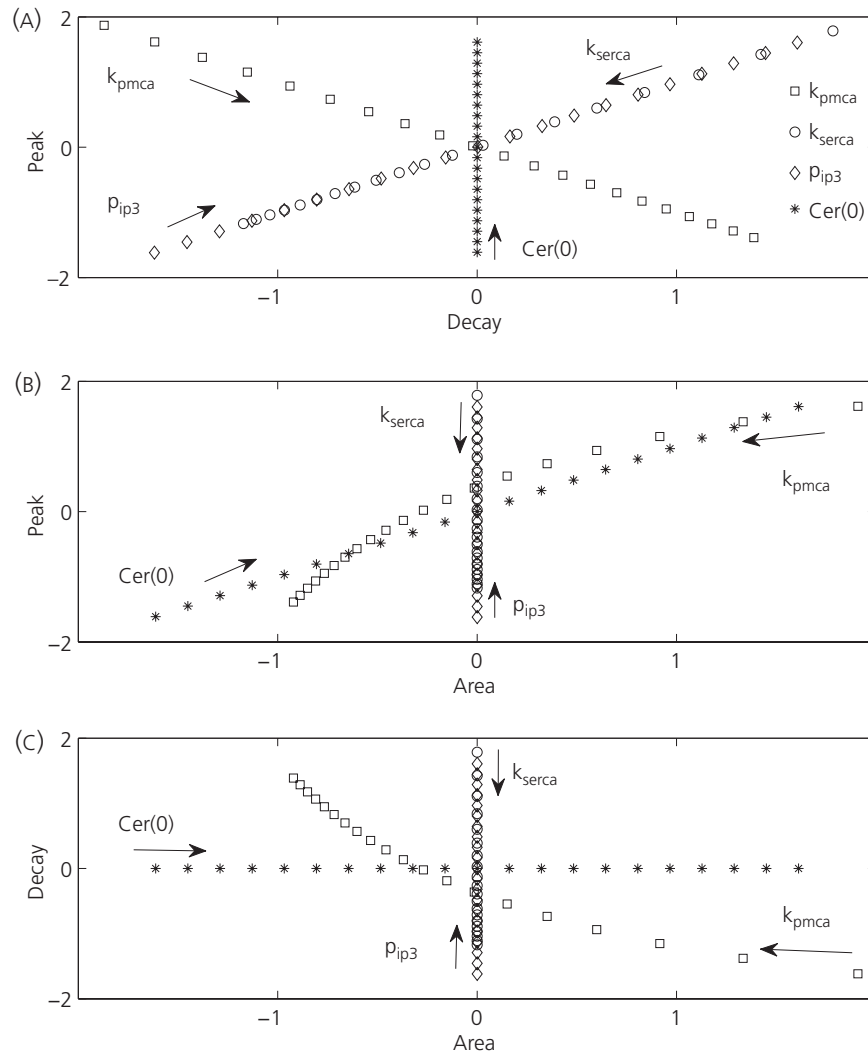


**Fig. 6.** Single parameter feature scatter plots. (A) Variation of different parameters produces different patterns in the peak-decay rate scatter plot. (B) Variation of  $k_{pmca}$  and  $C_{er}(0)$  cause a positive correlation between peak and area, whereas  $k_{serca}$  and  $p_{ip3}$  have no effect on the area. (C) Variation of  $C_{er}(0)$  has no effect on the decay rate,  $k_{serca}$  and  $p_{ip3}$  have no effect on the area, and  $k_{pmca}$  variation produces a negative correlation between decay rate and area.

negative slope, and some are vertical. Importantly, the pattern is a reflection of the parameter that is varied.

Next, we examine the scatter plot between peak and area (Fig. 6b). In this case, changing  $p_{ip3}$  and  $k_{serca}$  affects the value of the peak but not the area (because neither of these parameters appears in Eqn 15). Changes in  $C_{er}(0)$ , or in  $k_{pmca}$ , result in a positive correlation between area and peak, although with different slopes (both parameters appear in Eqns 14 and 15). In the area-peak feature space, no parameter introduces a negative correlation, so we should always expect either no correlation or a positive correlation between these two features.

The scatter plot between area and decay rate (Fig. 6c) reveals that changes in  $p_{ip3}$  and  $k_{serca}$  affect the decay rate but not the area. Conversely, changes in  $C_{er}(0)$  affect the area but not the decay rate. Finally, changing  $k_{pmca}$  results in a negative correlation between area and decay rate because changes in this parameter affect the decay rate more than the peak, resulting in higher peaks

having faster decays and consequently smaller areas. As a result, one should expect either no correlation or a negative correlation between these features.

In summary, variations in the different model parameters produce distinct patterns in the different slices (scatter plots) through feature space. The relationships (positive, negative or zero) of the scatter plot curves can be determined from the sensitivity analysis (Fig. 4) or, if available, from the analytical expressions for the different features.

### Multiple parameter variation

Here, we investigate the correlation patterns of the model feature scatter plots obtained by changing multiple parameters simultaneously, using the single parameter scatter plots to aid with the interpretation. We started by using equal variation in all the parameters. For each parameter, we selected a random value from a

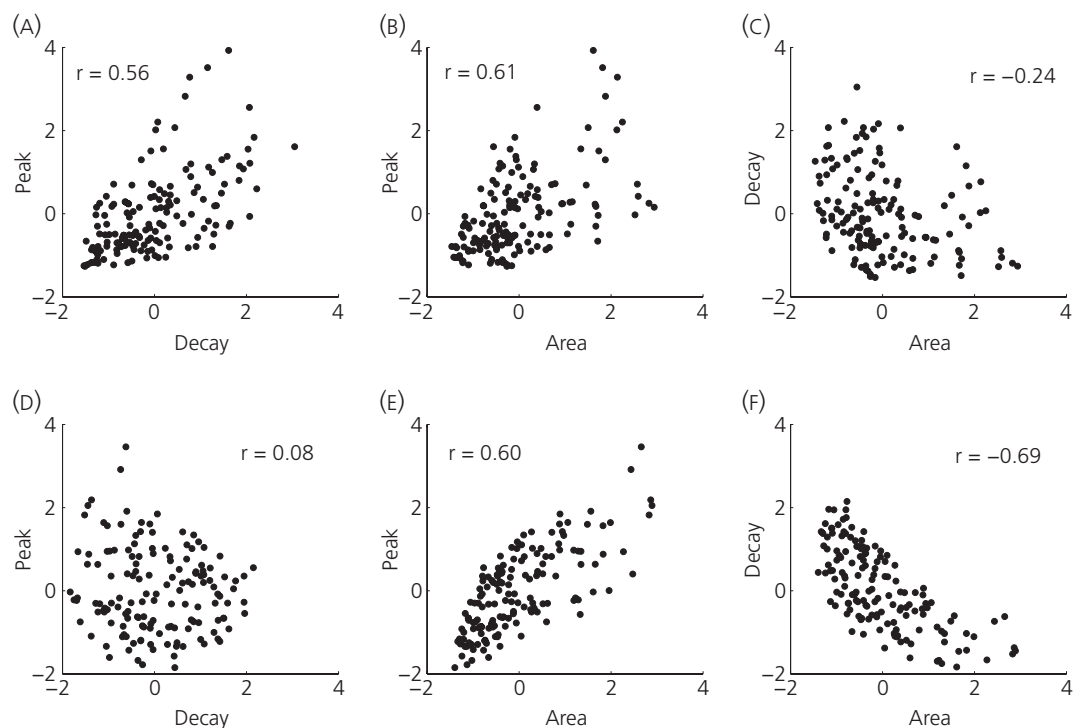


**Fig. 7.** Model scatter plots constructed by randomly drawing multiple parameter values. (A–C) All four model parameters are drawn from a uniform distribution spanning  $\pm 50\%$  of the default parameter value. (D–F) Parameter  $k_{pmca}$  is drawn from a uniform distribution that spans  $\pm 50\%$  of its default value, whereas all other parameters are drawn from a uniform distribution spanning  $\pm 25\%$  of their default parameter values.

uniform distribution that spans  $\pm 50\%$  of its default value. The results show a positive correlation in the decay rate against peak (Fig. 7A), and area against peak feature scatter plots (Fig. 7B). No correlation is found between decay rate and area (Fig. 7C). The single parameter correlation patterns in Fig. 6 help our understanding of how these multiple parameters correlations originate. The positive correlation between decay rate and peak (Fig. 7A) arises because changes in both  $k_{serca}$  and  $\rho_{ip3}$  give positive correlations, whereas only variation in  $k_{pmca}$  results in a negative correlation (Fig. 6A). The positive correlation between area and peak (Fig. 7B) arises because variation of all parameters gives either a positive correlation or no correlation (Fig. 6B). The absence of a correlation between area and decay rate (Fig. 7C) suggests that the influence of  $k_{pmca}$  variation (which would create a negative correlation) is dominated by the influence of variation in the other parameters (which results in no correlation) (Fig. 6C).

The feature scatter plots obtained from the model (Fig. 7A–C), however, are not in good agreement with the corresponding scatter plots obtained from the experimental data (Fig. 5). In both cases, there is a positive correlation between peak and area, although the experimental scatter plots show no correlation between decay rate and peak, and a negative correlation between area and decay rate. Analysis of the one parameter scatter plots (Fig. 6) suggests that increasing the variation in  $k_{pmca}$  relative to the variation of other parameters should remove the correlation between decay rate and peak and, at the same time, introduce a negative correlation between area and decay rate, as shown in Fig. 5.

Thus, we tested unequal variation in a different set of simulations. Parameters  $k_{serca}$ ,  $\rho_{ip3}$  and  $C_{er}(0)$  were chosen from a uniform distribution that spans  $\pm 25\%$  of the default parameter value. Parameter  $k_{pmca}$  was chosen from a wider uniform distribution spanning  $\pm 50\%$  of the default parameter value. The results of these simulations (Fig. 7D–F) show a good qualitative agreement with the experimental data. That is, in both model and experimental scatter plots, there was no correlation Fig. 7(D), a positive correlation in Fig. 7(E), and a negative correlation in Fig. 7(F).

Is a larger variation in  $k_{pmca}$  the only way to reproduce the correlation patterns, or can other combinations of parameters be found to achieve this? To check this, we used 10% or 50% variation of each parameter. Since there are four parameters [ $k_{pmca}$ ,  $k_{serca}$ ,  $\rho_{ip3}$  and  $C_{er}(0)$ ], there are sixteen possible combinations of small/large parameter variations.

In the first two combinations, all parameters are drawn from distributions with the same variation. We denote these as HHHH and LLLL, for high and low variation, respectively. The next sets of combinations consist of one of the four parameters being drawn from the high variation distribution and all the others from the low variation distribution (HLLL, LHLL, etc.). Next, we draw two parameters from the high distribution and two from the low distribution. Finally, three are drawn from the high distribution and one from the low distribution.

We present the results of these simulations using yet one more scatter plot, this time between two correlation values. We plotted together experimental data (Fig. 8, black triangles) and simulation

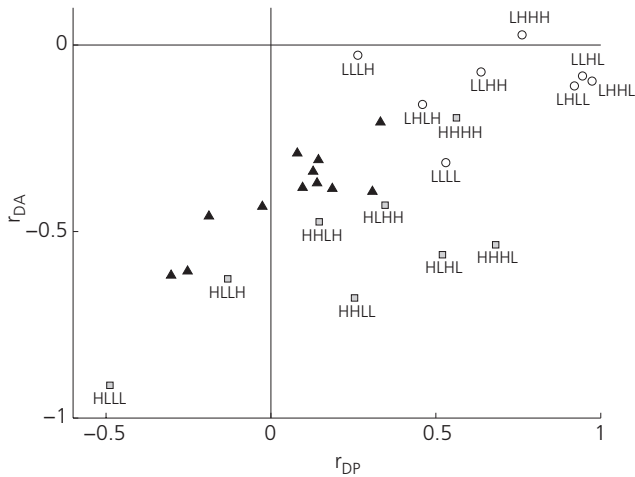


**Fig. 8.** Comparison between model and experimental results. The x-axis is the value of the correlation between peak and decay rate, the y-axis is the value of the correlation between decay and area. Labels H and L correspond to a parameter value drawn from a high ( $\pm 50\%$ ) and low ( $\pm 10\%$ ) variance distribution, respectively. The order of the parameters is  $k_{pmca}$ ,  $k_{serCa}$ ,  $\rho_{ip3}$ ,  $C_{er}(0)$ . Model simulations are divided in two categories: those in which at least  $k_{pmca}$  was chosen from a high distribution (grey filled squares) and all others (open circles). Model correlations are closer to experimental correlations (black filled triangles) when the value of  $k_{pmca}$ ,  $C_{er}(0)$  and one or no other parameter were drawn from the high variation distribution.

results (Fig. 8, squares and circles). The value of the correlation between decay rate and peak is on the horizontal axis, whereas the value of the correlation between area and decay rate is plotted on the vertical axis. Plotted this way, we see that the correlation pairs measured from the data lie almost on a line with positive slope. This line connects positive correlations on the horizontal axis and small negative correlations on the vertical axis with negative correlations on the horizontal axis and larger negative correlations on the vertical axis.

We distinguished between two categories in the simulations. First, there are simulations in which at least  $k_{pmca}$  was chosen from a high distribution (HLLL, HHLL, HHLL, etc.). These are the grey squares in Fig. 8. The open circles represent all other combinations (LLLL, LLLH, LLHH, etc.).

Comparison of model with experimental correlations shows that the agreement is best when  $C_{er}(0)$ ,  $k_{pmca}$  and another parameter have high variation. The points that most closely match the experimental results correspond to the HLLH, HHLH and HLHH combinations, all of which have a larger variation in  $k_{pmca}$  and  $C_{er}(0)$ . Thus, the analysis suggests that the most likely highly variable physical quantities in the lactotroph population used in these experiments are the plasma membrane pump rate and the level of  $Ca^{2+}$  concentration in the ER at the time of agonist application.

## Discussion

The goal of the present study was to evaluate the likely source of heterogeneity in the cytosolic  $Ca^{2+}$  response to  $Ca^{2+}$  mobilisation. We described a method that combines scatter plots from

experimental data with those made with a mathematical model. This allows the prediction of the primary source of heterogeneity. We illustrated the technique using the cytosolic  $Ca^{2+}$  response of pituitary lactotrophs to TRH challenge as a case study. From each  $Ca^{2+}$  trace, we extracted three features: the peak, the decay rate and the area under the curve. We found that  $k_{pmca}$  is one parameter that must vary across cells more than other parameters. This suggests that the  $Ca^{2+}$  extrusion pathway varies extensively among cells. Previous findings suggested that TRH may modulate the activity of the plasma membrane  $Ca^{2+}$  ATPase pump (36), which might contribute to the observed  $k_{pmca}$  heterogeneity.

We also found that variability in the  $Ca^{2+}$  concentration in the ER is likely a key element of heterogeneity in the response to TRH. This variability of  $[Ca^{2+}]_{ER}$  might be explained by the fact that cells that exhibit high degree of spontaneous activity would tend to have a higher ER  $Ca^{2+}$  level as a result of  $Ca^{2+}$  influx during electrical activity, as opposed to silent cells, which may have low ER  $Ca^{2+}$  level. The absence of dopamine inhibition in our *in vitro* conditions may increase the level of spontaneous activity (12, 19), which would allow the expression of the variability in the ER  $Ca^{2+}$  level.

In previous studies (17, 37), pituitary lactotrophs were challenged over a range of concentrations of TRH, essentially performing a sensitivity analysis. It was found that the peak of the  $Ca^{2+}$  response increases, up to a maximum, whereas, at the same time, the spike duration decreases. This relation between peak and spike duration corresponds to a positive correlation between peak and decay rate using the method we describe. Although this relationship is present in the single parameter sensitivity analysis of  $\rho_{ip3}$  (Fig. 6A), it does not appear in the peak versus decay rate scatter plot of the experimental data (Fig. 5A) or in the model scatter plot with non-uniform parameter variation (Fig. 7D). This apparent discrepancy is a result of the very large variation in  $Ca^{2+}$  mobilisation imposed by the range of TRH concentrations in (17, 37). This would be much larger than the natural variation occurring within a population of cells all exposed to the same dose of TRH. Thus, when looking at the results within a single dose of TRH, the positive correlation between peak and decay rate predicted by single parameter sensitivity analysis can be masked by variations in other parameters. This illustrates that, even when single parameter sensitivity analysis can be achieved experimentally, its results reveal little about the intrinsic heterogeneity within the cells.

In the data from different cells, all the parameters are varied at the same time, producing the observed variability. One way that mathematical models are sometimes adapted to such heterogeneous data is to adjust parameters so that the model output matches the mean of the experimental data. Another approach is to use a range of parameter values so that the distribution of model output matches the distribution of the experimental data. We use neither of these approaches; instead, we look at the qualitative relationships between features and determine which parameters must vary the most to reproduce these qualitative relations. We did so by drawing parameter values from a uniform distribution. Other distributions could be used, although the basic procedure would be the same. We assumed that the parameters of the

model were uncorrelated. That is, the biological components that the parameters represent are independent of each other. This may not be the case. For example, the expression levels of plasma membrane and SERCA pumps could be linked, so that cells would express high or low levels of both. To our knowledge, there are no data describing these linkages.

The model we used was simplified to derive analytical expressions, improving our understanding of the dynamics involved in the  $\text{Ca}^{2+}$  response to TRH. More complete mathematical models could be used, at the expense of more parameters. For example, one could incorporate a detailed description of all the intracellular events that take place from the binding of TRH to the opening of the  $\text{IP}_3$  receptors. These events include G-protein subunit dissociation, phospholipase C activation,  $\text{IP}_3$  formation and binding to receptors, and the gating of  $\text{IP}_3$  receptor-channels as a function of  $\text{Ca}^{2+}$  and  $\text{IP}_3$  concentrations. However, the results obtained so far suggest that variations in the  $\text{G}_q/\text{IP}_3$  pathway are not the main source of heterogeneity, otherwise the data would exhibit a positive correlation between peak and decay rate. Extensions of the model can be used to allow extracellular  $\text{Ca}^{2+}$  flux during agonist application, or consider other features such as the response latency. Extensions of this technique include other experiments and not only a more complex model. As a follow-up to our findings, one could challenge the lactotrophs with other stimulators. For example, one could briefly challenge the cells with potassium chloride. This would depolarise the membrane and open voltage-dependent  $\text{Ca}^{2+}$  channels, causing an increase in cytosolic  $\text{Ca}^{2+}$  that does not involve mobilisation from internal stores. In this way, one can produce a similar  $\text{Ca}^{2+}$  spike with a decaying phase that depends on a different set of parameters, but still includes  $k_{\text{pmca}}$ . This would allow the variability results from the TRH application to be tested against those from an independent source.

Finally, extensions may be considered to other biological systems. Relevant features (e.g. peak, decay rate and area) that are system specific must be identified first.

For example, pituitary gonadotrophs typically produce an oscillatory  $\text{Ca}^{2+}$  response to gonadotrophin-releasing hormone (38). If the agonist is applied in the absence of extracellular  $\text{Ca}^{2+}$ , the oscillations die out over time (38). Features that could be examined in this response are the oscillation period and amplitude and, if the experiment is performed in the absence of extracellular  $\text{Ca}^{2+}$ , the number of oscillations produced. Although the features differ from those in the present study, the approach used to investigate likely sources of heterogeneity would be the same.

## Acknowledgements

We thank Marc Freeman for providing many insightful comments on this manuscript and Takafumi Inoue for kindly providing the  $\text{Ca}^{2+}$  imaging software TI WORKBENCH. This research was supported by NIH grants DA-19356 and DK-43200.

Received 7 May 2010,  
revised 14 July 2010,  
accepted 20 August 2010

## References

- 1 Alvarez-Buylla A, Kohwi M, Nguyen TM, Merkle FT. The heterogeneity of adult neural stem cells and the emerging complexity of their niche. *Cold Spring Harb Symp Quant Biol* 2008; **73**: 357–365.
- 2 Salk JJ, Fox EJ, Loeb LA. Mutational heterogeneity in human cancers: origin and consequences. *Annu Rev Pathol* 2010; **5**: 51–75.
- 3 Cleaver JE, Lam ET, Revet I. Disorders of nucleotide excision repair: the genetic and molecular basis of heterogeneity. *Nat Rev Genet* 2009; **10**: 756–768.
- 4 McArdle CA, Evans JJ. The circus in the pituitary. *Trends Endocrinol Metab* 2001; **12**: 429–430.
- 5 Kærn M, Elston TC, Blake WJ, Collins JJ. Stochasticity in gene expression: from theories to phenotypes. *Nat Rev Gen* 2005; **6**: 451–464.
- 6 Evans JJ. The anterior pituitary gland is mysterious, alluring and useful. *Arch Physiol Biochem* 2002; **110**: 3–8.
- 7 Van Goor F, Zivadinovic D, Stojilkovic SS. Differential expression of ionic channels in rat anterior pituitary cells. *Mol Endocrinol* 2001; **15**: 1222–1236.
- 8 Wilkinson DJ. Stochastic modeling for quantitative description of heterogeneous biological systems. *Nat Rev Gen* 2009; **10**: 122–133.
- 9 Chung JD, Stephanopoulos G. On physiological multiplicity and population heterogeneity of biological systems. *Chem Eng Sci* 1996; **51**: 1509–1521.
- 10 Li X, Zhang J, Small M. Self-organization of a neural network with heterogeneous neurons enhances coherence and stochastic resonance. *Chaos* 2009; **19**: 013126.
- 11 Kitano H. Biological robustness. *Nature* 2004; **5**: 826–837.
- 12 Ho MY, Kao JPY, Gregerson KA. Dopamine withdrawal elicits prolonged calcium rise to support prolactin rebound release. *Endocrinology* 1996; **137**: 3513–3521.
- 13 Winiger BP, Schlegel W. Rapid transient elevations of cytosolic calcium triggered by thyrotropin releasing hormone in individual cells of the pituitary line GH<sub>3</sub>B<sub>6</sub>. *Biochem J* 1988; **255**: 161–167.
- 14 Winiger BP, Wuarin F, Zahnd GR, Wollheim CB, Schlegel W. Single cell monitoring of cytosolic calcium reveals subtypes of rat lactotrophs with distinct responses to dopamine and thyrotropin-releasing hormone. *Endocrinology* 1987; **121**: 2222–2228.
- 15 Castaño JP, Kineman RD, Frawley LS. Dynamic monitoring and quantification of gene expression in single, living cells: a molecular basis for secretory cell heterogeneity. *Mol Endocrinol* 1996; **10**: 599–605.
- 16 De Paul AL, Pons P, Aoki A, Torres AL. Heterogeneity of pituitary lactotrophs: immunocytochemical identification of functional subtypes. *Acta Histochem* 1997; **99**: 277–289.
- 17 Ashworth R, Hinkle PM. Thyrotropin-releasing hormone-induced intracellular calcium responses in individual rat lactotrophs and thyrotrophs. *Endocrinology* 1996; **12**: 5205–5212.
- 18 Lledo PM, Guerineau N, Mollard P, Vincent JD, Israel JM. Physiological characterization of two functional states in subpopulations of prolactin cells from lactating rats. *J Physiol* 1991; **437**: 477–494.
- 19 Israel JM, Kirk C, Vincent JD. Electrophysiological responses to dopamine of rat hypophysial cells in lactotroph-enriched primary cultures. *J Physiol* 1987; **390**: 1–22.
- 20 Shorte SL, Faught WJ, Frawley LS. Spontaneous calcium oscillatory patterns in mammatropes display non-random dynamics. *Cell Calcium* 2000; **28**: 171–179.
- 21 Reid G, Bauer CK, Bunting R, Mason WT, Schwarz JR. Most lactotrophs from lactating rats are able to respond to both thyrotropin-releasing hormone and dopamine. *Mol Cell Endocrinol* 1996; **124**: 121–129.
- 22 Zhang J, Chen C, Kukstas LA, Vincent JD, Israel JM. Functional lactotroph heterogeneity in lactating rats and *in vitro* modification by 17beta-estradiol. *J Neuroendocrinol* 1990; **2**: 815–823.

- 23 De Paul A, Pons P, Aoki A, Torres A. Different behavior of lactotroph cell subpopulations in response to angiotensin II and thyrotrophin-releasing hormone. *Cell Mol Neurobiol* 1997; **17**: 245–258.
- 24 Velkeniers B, Kazemzadeh M, Vanhaelst L, Hooghe-Peters EL. Functional heterogeneity with respect to oestrogen treatment in prolactin cell subpopulations separated by Percoll gradient centrifugation. *J Endocrinol* 1994; **141**: 251–258.
- 25 Burris TP, Freeman ME. Low concentrations of dopamine increase cytosolic calcium in lactotrophs. *Endocrinology* 1993; **133**: 63–68.
- 26 Hinkle PM, Nelson EJ, Ashworth R. Characterization of the calcium response to thyrotropin-releasing hormone in lactotrophs and GH cells. *Trends Endocrinol Metab* 1996; **10**: 370–374.
- 27 Albert PR, Tashjian AH. Relationship of thyrotropin-releasing hormone-induced spike and plateau phases in cytosolic free  $\text{Ca}^{2+}$  concentrations to hormone secretion. *J Biol Chem* 1984; **259**: 15350–15363.
- 28 Tabak J, Gonzalez-Iglesias AE, Toporikova N, Bertram R, Freeman ME. Variations in the response of pituitary lactotrophs to oxytocin during the rat estrous cycle. *Endocrinology* 2010; **151**: 1806–1813.
- 29 Velkeniers B, Hooghepeters EL, Hooghe R, Belayew A, Smets G, Claeys A, Robberecht P, Vanhaelst L. Prolactin cell subpopulations separated on discontinuous Percoll gradient – An immunocytochemical, biochemical, and physiological characterization. *Endocrinology* 1988; **123**: 1619–1630.
- 30 Koshimizu T, Tomic M, Wong AOL, Zivadinovic D, Stojilkovic SS. Characterization of purinergic receptors and receptor-channels expressed in anterior pituitary cells. *Endocrinology* 2000; **141**: 4091–4099.
- 31 Bertram R, Sherman A. Filtering of calcium transients by the endoplasmic reticulum in pancreatic  $\beta$ -cells. *Biophys J* 2004; **87**: 3775–3785.
- 32 Fiekers JF. The contribution of plasma membrane  $\text{Na}^+$ - $\text{Ca}^{2+}$  -exchange and the  $\text{Ca}^{2+}$  -ATPase to the regulation of cytosolic calcium ( $[\text{Ca}^{2+}]_i$ ) in a clonal pituitary cell line (AtT-20) of mouse corticotropes. *Life Sci* 2001; **70**: 681–698.
- 33 Ermentrout GB. *Simulating, Analyzing, and Animating Dynamical Systems: A Guide to XPPAUT for Researchers and Students*. Philadelphia, PA: SIAM, 2002.
- 34 Bertram R, Arceo RC II. A mathematical study of the differential effects of two SERCA isoforms on  $\text{Ca}^{2+}$  oscillations in pancreatic islets. *Bull Math Biol* 2008; **70**: 1251–1271.
- 35 Yu R, Hinkle P. Desensitization of thyrotropin-releasing hormone receptor-mediated response involves multiple steps. *J Biol Chem* 1997; **272**: 28301–28307.
- 36 Nelson EJ, Hinkle PM. Thyrotropin-releasing hormone activates  $\text{Ca}^{2+}$  efflux. *J Biol Chem* 1994; **49**: 30854–30860.
- 37 Nelson EJ, Hinkle PM. Characteristics of the  $\text{Ca}^{2+}$  spike and oscillations induced by different doses of thyrotropin-releasing hormone (TRH) in individual pituitary cells and nonexcitable cells transfected with TRH receptor complementary deoxyribonucleic acid. *Endocrinology* 1994; **3**: 1084–1092.
- 38 Stojilkovic SS, Kukuljan M, Ida T, Rojas E, Catt KJ. Integration of cytoplasmic calcium and membrane potential oscillations maintains calcium signaling in pituitary gonadotrophs. *Proc Natl Acad Sci USA* 1992; **89**: 4081–4085.